Solar Energy Materials & Solar Cells 136 (2015) 148–156

Contents lists available at ScienceDirect

Solar Energy Materials & Solar Cells

journal homepage: www.elsevier.com/locate/solmat

Bimodally dispersed silver paste for the metallization of a crystalline silicon solar cell using electrohydrodynamic jet printing

Dong-Youn Shin [a,*], Jun-Young Seo [a], Hyowon Tak [b], Doyoung Byun [c]

[a] Department of Graphic Arts Information Engineering, Pukyong National University, 365, Sinseon-ro, Nam-gu, Busan 608-739, Republic of Korea
[b] Enjet Inc., Ltd., 2066, Seobu-ro, Jangan-gu, Suwon-si, Gyeonggi-do 440-746, Republic of Korea
[c] Department of Mechanical Engineering, Sungkyunkwan University, 2066, Seobu-ro, Jangan-gu, Suwon-si, Gyeonggi-do 440-746, Republic of Korea

ARTICLE INFO

Article history:
Received 5 August 2014
Received in revised form
28 December 2014
Accepted 6 January 2015

Keywords:
Bimodal dispersion
Silver paste
Electrohydrodynamic jet printing
Metallization
Silicon solar cell

ABSTRACT

Conventional silver paste for crystalline silicon solar cells exhibits low cell efficiency when deposited by non-contact electrohydrodynamic jet printing because of either high volumetric shrinkage or low packing density when there is no printing pressure applied to the silver paste. Therefore, we develop bimodally dispersed silver paste for electrohydrodynamic jet printing to resolve both volumetric shrinkage and packing density of the conventional silver paste, and its electrical and rheological traits are investigated. The bimodally dispersed silver paste exhibits lower unit-line resistance, which is inversely proportional to the weight ratio of small-to-large silver particles due to the increased packing density, and higher contact resistivity above a certain weight ratio for small-to-large silver particles. This behaviour results from the obstructed melt flow of glass frit by the early coarsened and densified small silver particles at an elevated temperature. The increased weight ratio of the small particles also raises the viscosity of the bimodally dispersed silver paste above the point where electrohydrodynamic jet printing is possible. By employing a binary solvent mixture and metallorganic silver as a viscosity reducing agent, the bimodally dispersed silver paste is tuned for electrohydrodynamic jet printing, and the front-side metallization of a polycrystalline silicon solar cell with the emitter sheet resistance of 60 Ω/sq is constructed. With the abnormally high aspect ratio of silver electrodes at 0.86, a cell efficiency of 16.72% is achieved, which is higher than that of screen-printed cells with the similar emitter sheet resistance by +0.22–0.52%p.

1. Introduction

The global market of crystalline silicon solar cells has demanded higher cell efficiency at a lower manufacturing cost because of the intensive pressure related to the severe manufacturing capacity surplus of crystalline silicon solar cells worldwide [1]. To reduce manufacturing cost, the thickness of crystalline silicon solar cell wafers has been reduced from 370 μm to 180 μm since 1997; the thickness is predicted to be less than 150 μm in the near future [2]. To employ thinner crystalline silicon solar cell wafers, various non-contact printing techniques such as aerosol jet printing [3,4], piezoelectric drop-on-demand (DOD) ink-jet printing [5–7], and dispensing printing [8–10] have been explored to replace the current screen-printing technique.

Aerosol jet printing utilizes a jet stream focused by a sheath gas from the concentric outer nozzle, and silver electrodes could be formed as fine as 14 μm in width [3]. However, the typical thickness of silver electrodes after the firing process does not exceed 2 μm [4], and a sophisticated additional process, *i.e.*, light induced plating, is required to thicken the silver electrodes [11]. One typical problem at occurs as a result of the light induced plating process is that the electroplated silver electrodes are not only thickened but also widened. In particular, the increase in the width is approximately two times the increase in the thickness of the silver electrodes.

Direct front-side metallization of the silver electrodes was demonstrated using piezoelectric DOD ink-jet printing. However, the use of silver nanoparticles, which are capped with a polymeric dispersant, induces high volumetric shrinkage during the firing process because of the high volume ratio of the dispersant to the silver nanoparticles. Consequently, poor contact formation between the silver electrodes and the emitter layer of the crystalline silicon solar cell leads to a low cell efficiency of 12.1% [7].

Dispensing printing has been the most successful non-contact printing technique because it does not require a sophisticated additional process to thicken the silver electrodes. Moreover, the achieved cell efficiency of a polycrystalline silicon solar cell was as

* Corresponding author. Tel.: +82 51 629 6394; fax: +82 51 629 6388.
E-mail addresses: dongyoun.shin@gmail.com (D.-Y. Shin), iceblu2@gmail.com (J.-Y. Seo), hwtak@enjet.co.kr (H. Tak), dybyun@skku.edu (D. Byun).

http://dx.doi.org/10.1016/j.solmat.2015.01.008
0927-0248/

high as 16.77% [8], which is not only comparable to that of a screen-printed cell but also the highest among directly metallized polycrystalline silicon solar cells produced using non-contact printing techniques. However, the issue of nozzle clogging in dispensing printing would be is a persistent problem because the construction of fine silver electrodes is strongly dependent on the nozzle diameter.

Electrohydrodynamic (EHD) jet printing has recently attracted attention as an alternative to the aforementioned non-contact printing techniques. It has a very unique ability to produce ultra-fine patterns with either an ultra-fine nozzle [12,13] or a large diameter nozzle [14]. Moreover, EHD jet printing can directly print fine conductive lines with an abnormally high aspect ratio [15]. Various sizes of silver particles can be employed unlike piezo-electric DOD ink-jet printing or dispensing printing because EHD jet printing can construct fine conductive lines with a large diameter nozzle. It can also employ moderately viscous silver paste, which is not possible with piezoelectric DOD ink-jet printing.

Despite all of these distinctive features of EHD jet printing, the cell efficiency of a polycrystalline silicon solar cell metallized with EHD jet printing remained as low as 13.7% when commercially available silver paste for screen-printing was used after dilution [15]. In contrast, the cell efficiency of a polycrystalline silicon solar cell metallized with screen-printing was 16.2% with the same silver paste. This discrepancy implies that the simple dilution of silver screen-printing paste is not effective for EHD jet printing in solar cell applications.

Therefore, this study primarily focuses on the development of silver paste for EHD jet printing in the front-side metallization of a crystalline silicon solar cell. With respect to the smooth flow of silver paste through the nozzle, the use of small silver particles is certainly beneficial, but it could also affect the sound contact formation between the silver electrodes and the emitter layer of a crystalline silicon solar cell. To evade the detrimental effects of small silver particles on the contact formation, we consider a bimodal dispersion of small and large silver particles, and the influence of the bimodal dispersion of silver particles on the electrical characteristics such as unit-line resistance and contact resistivity will be investigated. In addition, an effective means for controlling the viscosity of the bimodally dispersed silver paste for EHD jet printing without significantly altering the solid content of the paste will be introduced. Finally, the cell efficiency of a polycrystalline silicon solar cell metallized with EHD jet printing will be presented and compared with that of screen-printed cells.

2. Experimental

The in-house-developed bimodally dispersed silver paste for EHD jet printing was composed of (1) small (HP-0702, D50 = 0.13–0.35 μm, Heesung Metal Ltd., Republic of Korea) and large silver particles (HP-0710, D50 = 0.9–1.4 μm, Heesung Metal Ltd., Republic of Korea), as shown in Fig. 1(a) and (b); (Fig. 2) glass frit (V2172, D50 ≈ 4.52 μm, Ceradyne Inc., USA), as shown in Fig. 1(c); (Fig. 3) a dispersant (Zephrym PD 2246 SF, Croda International Plc., UK); (4) an organic binder (ethyl cellulose, CAS No. 9004-57-3, Order No. 200646 for low molecular weight or order No. 200654 for high molecular weight, Sigma-Aldrich Corp., USA); (5) a carrier vehicle made with butyl carbitol acetate (BCA) (2-(2-butoxyethoxy) ethyl acetate, CAS No. 124-17-4, Samchun Pure Chemical Co., Ltd., Republic of Korea), xylene (*o*-xylene, CAS No. 95-47-6, SK Chemicals Co., Ltd., Republic of Korea) and/or α-terpineol (CAS No. 98-55-5, Kanto Chemical Co., Inc., Japan); and (6) metallorganic silver (CXSV060, Gelest Inc., USA) as an additive to adjust the viscosity of the bimodally dispersed silver paste.

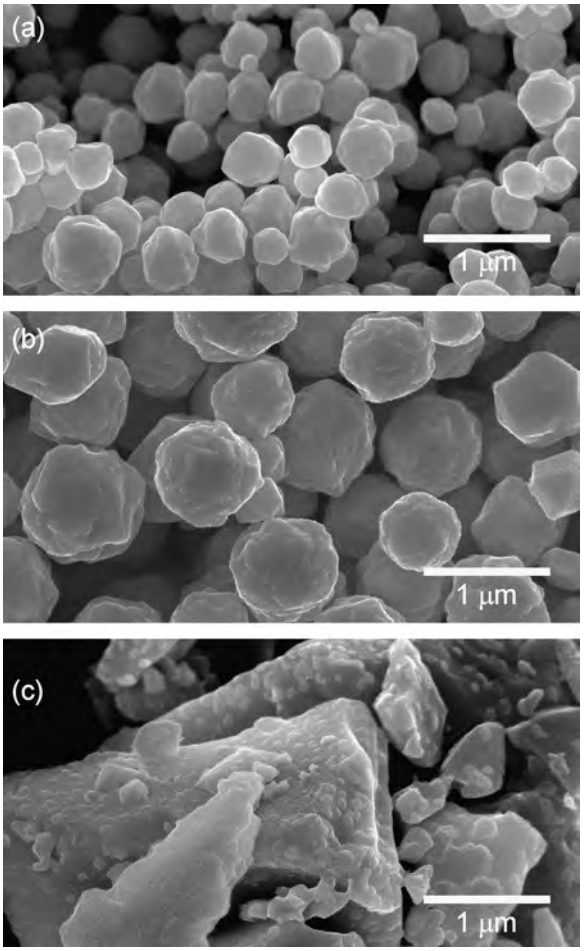

Fig. 1. Microscopic images of the used silver particles and glass frit: (a) small silver particles (HP-0702), (b) large silver particles (HP-0710), and (c) glass frit (V2172).

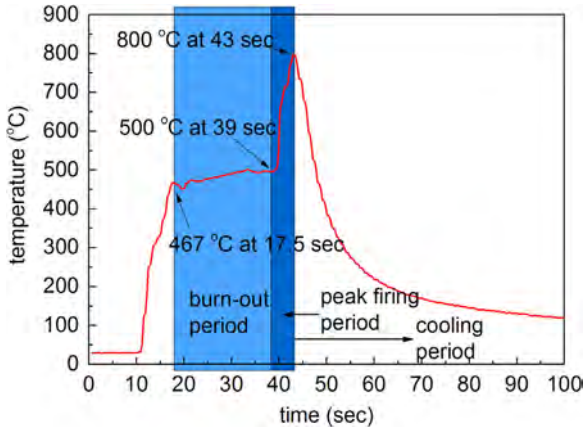

Fig. 2. The exemplary thermal profile used for the high-temperature firing process.

For the formulation of the bimodally dispersed silver paste, the organic binder, dispersant, and metallorganic silver were dissolved in the carrier vehicle, and the mixture was stirred overnight on a hot plate stirrer (DH.WMH03506, DAIHAN Scientific Co., Ltd., Republic of Korea) at the temperature and stirring speed of 70 °C and 700 rpm, respectively. Then, silver particles and as-received glass frit were pre-dispersed into the prepared carrier vehicle using a planetary centrifugal mixer (ARE-310, Thinky Corp., Japan). After removing the air bubbles in a vacuum desiccator (VDC-41U, Jeio Tech Co., Ltd., Republic of Korea) for 1 h, the bimodally dispersed silver paste was processed with a three-roll mill (EXAKT

50, EXAKT Advanced Technologies GmbH, Germany) for 3 min and was returned to the vacuum desiccator for 1 h. For stabilizing the bimodally dispersed silver paste, the paste was placed on a roll mixer (10 roll mixer, Hwashin Technology Co., Republic of Korea) at the speed of 40 rpm for three days. The total solid content of silver particles and glass frit in the bimodally dispersed silver paste was controlled to the 84–85 wt% range.

For electrical characterization of the bimodally dispersed silver paste, specimens with equidistant linear silver electrodes were prepared with 2-mm line spacing using screen-printing on textured monocrystalline silicon wafers with the topmost layer consisting of SiN_x (50 Ω/sq emitter sheet resistance, KPE Co., Ltd., Republic of Korea). The as-printed specimens were dried on a hot plate stirrer at 110 °C for 10 min, followed by a second drying on a hot plate (DHSL.HP2020300, DHSL Korea Co., Ltd., Republic of Korea) at 150 °C for 10 min. The dried specimens were subjected to a high-temperature firing process using a rapid thermal processor (AccuThermo AW 610, Allwin21 Corp., USA). The typical thermal profile used in this study is shown in Fig. 2, where only the peak firing temperature was changed. For characterizing the contact resistivity, the three-point probe method was employed using a probe station (MST 4000 A, MS Tech Co., Ltd., Republic of Korea) and a source meter (Model 2401, Keithley Instruments Inc., USA) [16–18]. The same experimental set-up was employed to measure the unit-line resistance of silver electrodes with four-point probes.

An optical microscope (JSZ-7XT, Samwon Scientific Ind. Co., Ltd., Republic of Korea) was used to measure the line width of the silver electrodes. The microscopic images were taken using a field-emission scanning electron microscope (FE-SEM) (JSM-6700 F, Jeol Ltd., Japan or SUPRA-55VP, Carl Zeiss NTS GmbH, Germany). A rheometer (RheoScope 1, Thermo Fisher Scientific Inc., Germany) was used to measure the viscosity of the bimodally dispersed silver paste with a cone-plate sensor, C60/1° Ti PO, at 23 °C. To avoid the uncertainties of the measured viscosity values due to the strong hysteretic behaviours of the developed silver paste, the viscosity measurements were done at the shear strain rate of 100 s^{-1} in 10 s after the rotation of a cone-plate sensor, when the deviation of the measured viscosity values became less than 5%.

For the EHD-jetting tests and the fabrication of a polycrystalline silicon solar cell, a standard version of the eNano printer (Enjet Co., Republic of Korea) was used, as shown in Fig. 3. The used eNano printer consisted of a 100-μm diameter ceramic nozzle, a high voltage supply unit, a micro-syringe pump, a CCD camera, an *x*–*y*–*z* axis motion unit, and a substrate unit on which an aluminium platen was laid as a counter electrode. High voltage is applied across the nozzle and the counter electrode, while a liquid is pumped through the nozzle. The electric charge on the liquid meniscus develops an electric stress. If this electric stress exceeds surface tension and viscous force of the liquid meniscus, then the liquid meniscus is elongated along the electric field direction, and forms a conical shape, known as a Taylor cone, from which a stable continuous jet of liquid can be emitted [19]. Consequently, the most critical parameter to control in silver paste is viscosity rather than surface tension since the viscous force of a thick paste is generally much larger than its surface tension.

3. Results and discussion

3.1. Bimodal dispersion of silver particles

As an empirical rule of thumb, the particle size should be approximately one-hundredth of the nozzle diameter to evade nozzle clogging [20]. Though EHD jet printing potentially has fewer nozzle clogging problems than piezoelectric DOD ink-jet printing due to its unique capability for printing fine conductive lines with a relatively large diameter nozzle, the use of small silver particles might be deemed equally beneficial in terms of smooth nozzle flow. However, the use of extremely small silver particles, *i.e.*, silver nanoparticles, was found to have a detrimental effect on the contact formation between the silver electrodes and the emitter layer of the crystalline silicon solar cell [7]. If the thickness of the dispersant layer is 2.5 nm, the volume ratio of the dispersant to an 18.1-nm-diameter silver nanoparticle reaches as high as 107.87 vol%. This remarkably high dispersant-to-silver nanoparticle volume ratio eventually caused strong mechanical stress during firing due to the significant volumetric shrinkage and resulted in poor contact formation [7]. In contrast, the volume ratio of the dispersant to the used small or large silver particles in this study lay in the range of 1.08 vol% and 11.99 vol%, and no delamination issues were observed at the contact

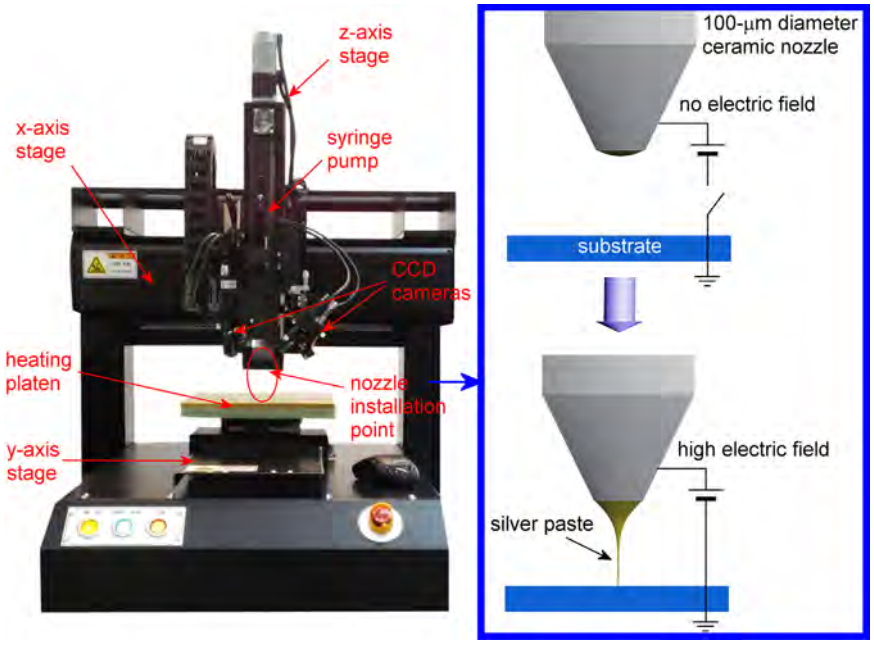

Fig. 3. Standard version of the eNano printer for EHD jet printing.

interface between the silver electrodes and the emitter layer of the crystalline silicon solar cell. The evasion of poor contact formation occurred because the volumetric shrinkage due to the volume ratio of the dispersant to the used small or large silver particles is practically much smaller than the volume fraction of the voids in the case of monodispersed silver particles, 36 vol% [21].

Note that the diluted version of the conventional silver paste for EHD jet printing could not achieve cell efficiency comparable to that of screen-printed cells, even though the composition of the silver paste was not affected by the dilution process [15]. This low cell efficiency with EHD jet printing occurs due to the absence of printing pressure that fails to produce as-printed silver electrodes with high packing density, which can be readily achieved with the printing pressure applied by a squeegee in screen-printing. Because the voids between the silver particles have no affirmative contribution to the electrical characteristics, we want to fill the voids between the silver particles with smaller silver particles. When the size and weight ratios of the small-to-large silver particles are set around 1 to 7, and 15 to 85, respectively, the minimum volume fraction of voids is as low as 15 vol%, which is considerably lower (21 vol%p) than the case of monodispersed silver particles [21]. Therefore, the bimodal dispersion of silver particles could be hypothesized to have an affirmative effect on the electrical characteristics of the silver electrodes, such as the unit-line resistance and contact resistivity.

To verify this hypothesis, small silver particles were mixed with large silver particles at different weight ratios from 5 wt% to 25 wt%, while the solid content of glass frit was maintained at 3 wt% with respect to the silver particles. Though the microscopic cross-sectional images of the fired silver electrodes in Fig. 4show no notable difference between samples with different weight ratios of small-to-large silver particles, the decrease in the unit-line resistance is evident, as shown in Fig. 5(a).

In contrast to the assertion by Hilali et al. that the use of smaller silver particles leads to higher contact resistivity [22], the contact resistivity of the bimodally dispersed silver paste exhibits a minimum contact resistivity at the small-to-large silver particle weight ratio of 15 wt%. The decrease of the contact resistivity up to

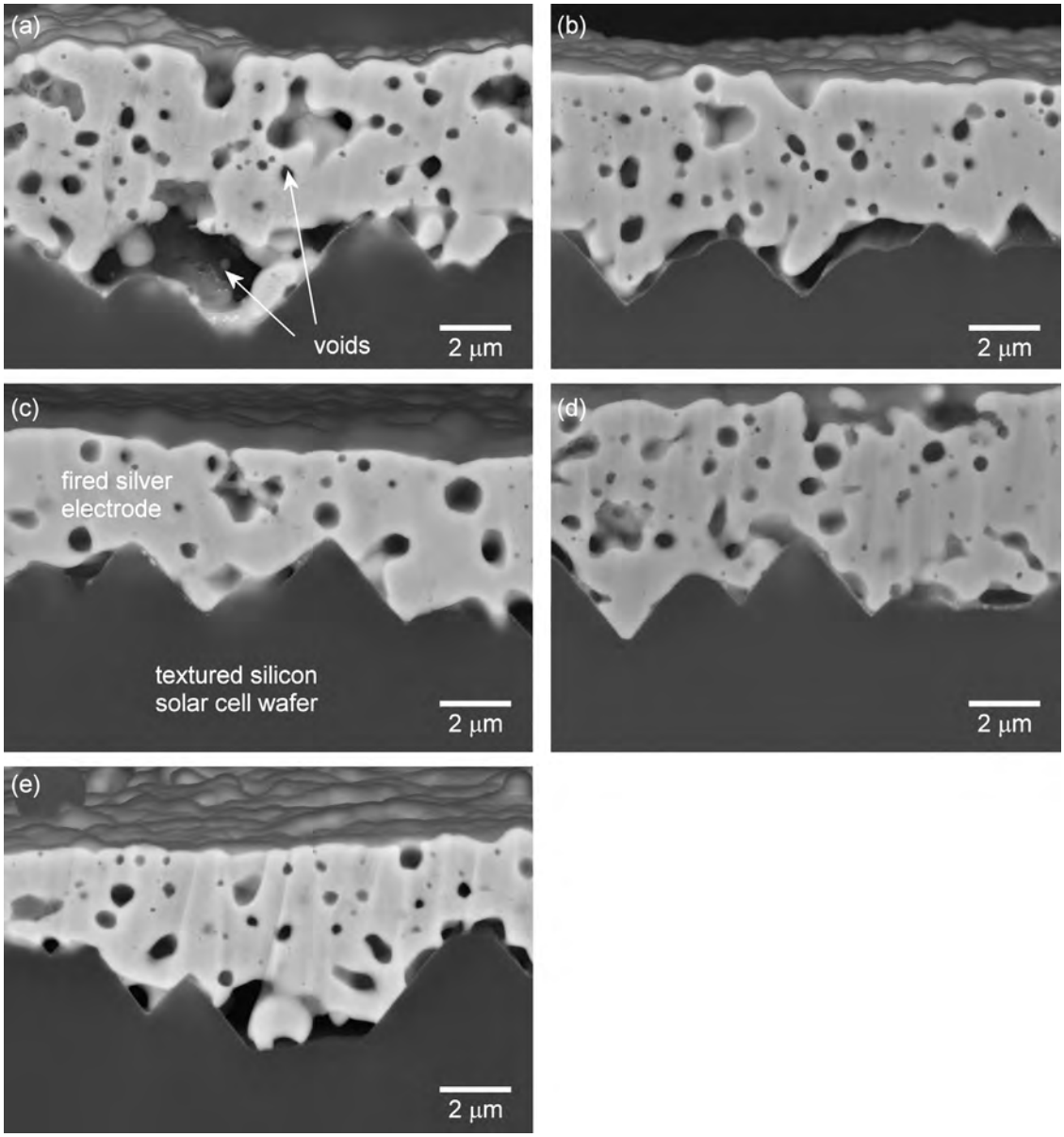

Fig. 4. Microscopic cross-sectional images of the fired silver electrodes at different weight ratios of small-to-large silver particles: (a) 5 wt%, (b) 10 wt%, (c) 15 wt%, (d) 20 wt%, and (e) 25 wt%.

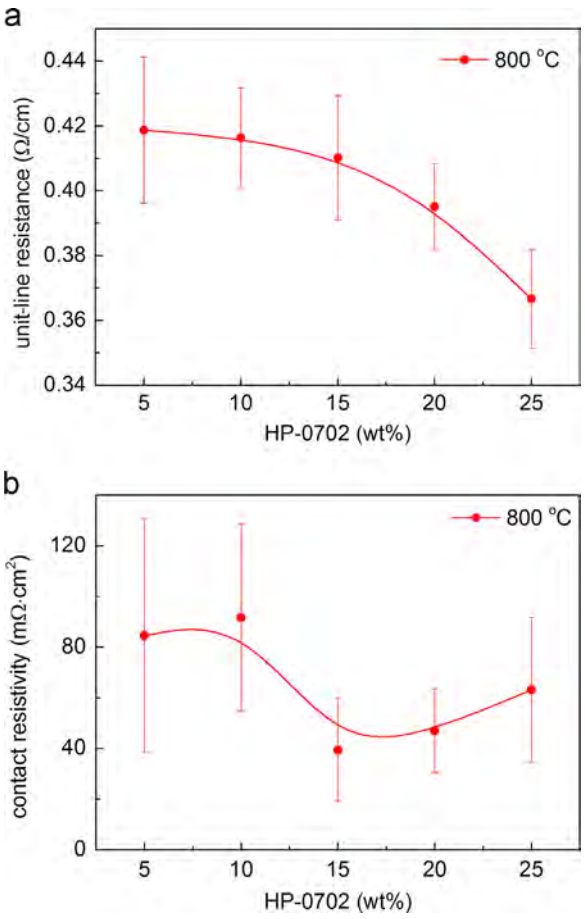

Fig. 5. Influence of the weight ratio of the small (HP-0702) to large silver particles (HP-0710) on (a) unit-line resistance and (b) contact resistivity.

the small-to-large silver particle weight ratio of 15 wt% might be explained by two factors. First, the capillary force-driven melt flow of the glass frit could be facilitated by the inclusion of small silver particles [23] with the assumption that glass frit easily wets silver particles. Consequently, the glass frit melt readily migrates to the contact interface between the silver electrodes and the emitter layer of the crystalline silicon solar cell and contributes to low contact resistivity. However, the capillary force-driven melt flow of the glass frit cannot explain why contact resistivity increases at the small-to-large silver particle weight ratio above 15 wt%. Therefore, we postulate a new hypothesis that the melt flow of the glass frit is actually governed by the squeezing force of the silver particles through their coarsening and densification.

As bridges form between silver particles at an elevated temperature, the melt of glass frit must be squeezed by the densification and coarsening of silver particles, as shown in Fig. 6(b). Because the inclusion of small silver particles facilitates the densification and coarsening of silver particles, the melt of glass frit can migrate to the contact interface and contribute to the low contact resistivity. However, if the weight ratio of small silver particles exceeds 15, the coarsening and densification of small silver particles causes the passage between silver particles to narrow, subsequently impeding the melt flow of glass frit. As a result, some of the glass frit could be trapped, as shown in Fig. 6(c). Because a smaller amount of glass frit reaches the SiN_x layer (Fig. 4(e)), a sound contact formation cannot be made, resulting in an increase of the contact resistivity for weight ratios of small-to-large silver particles above 15 wt%.

Because both the unit-line resistance and contact resistivity simultaneously contribute to the series resistance, a trade-off on the weight ratio of small-to-large silver particles must be made, and the weight ratio of small-to-large silver particles was decided to be 20 wt%. After determining the weight ratio, the solid content of glass frit was optimized by measuring the contact resistivity at two different peak firing temperatures: 780 °C and 800 °C. The used glass frit in the bimodally dispersed silver paste exhibited the minimum contact resistivity at 11 wt% with respect to the bimodal dispersed silver particles when fired at 780 °C, as shown in Fig. 7. Hereinafter, the solid content of glass frit in the bimodally dispersed silver paste was maintained at 11 wt% with respect to the bimodally dispersed silver particles.

3.2. Optimal viscosity range of the bimodally dispersed silver paste for EHD jet printing

To determine the optimal viscosity range of the bimodally dispersed silver paste for EHD jet printing, a series of dummy inks containing ethyl cellulose (CAS No. 9004-57-3, Order No. 200654, Sigma-Aldrich Corp., USA) at different concentrations in BCA were formulated, and the viscosities are plotted in Fig. 8, where the shear strain rate and temperature were set to 100 s^{-1} and 23 °C, respectively.

If the ink viscosity was too low (around 590 cP or below), it was found through EHD-jetting tests that dripping occurred at low frequency, and hence no continuous lines were printed, as shown in Fig. 9(a). At slightly higher ink viscosity (from 880 cP to 1800 cP), unstable jet spinning appeared. In contrast, at very high ink viscosity (around 6000 cP and above), ink was forced out by the syringe pump in a process similar to dispensing printing without the formation of a Taylor cone at the nozzle tip. However, when the ink viscosity fell in the 2200–4200 cP range, a stable Taylor cone was formed at the nozzle tip, and continuous lines were printed, as shown in Fig. 9(b).

However, the viscosity of the bimodally dispersed silver paste abruptly increased with the solid content increase of small silver particles at around 10 wt%, as shown in Fig. 10(a). Although the viscosity of the bimodally dispersed suspension is known to decrease under certain conditions such as specific diameter and volume ratios of small and large particles [24], the solid content increase of small silver particles in the developed bimodally dispersed silver paste generally tends to increase the viscosity. This velocity increase occurs because the high specific surface area of small silver particles leads to an interaction between the particles and organic species in the bimodally dispersed silver paste. To formulate the bimodally dispersed silver paste with a sufficiently high solid content that is also within the EHD-jettable viscosity range, three conventional measures were taken. First, the concentration of the organic binder is decreased to the point where no cracks appear in the dried silver electrodes. Another technique is to use a low-molecular-weight organic binder in place of a high-molecular-weight organic binder because the ink viscosity tends to be proportional to the organic binder molecular weight. Finally, a binary solvent mixture is employed as a carrier vehicle to increase the solubility of the organic binder. To easily identify the influence of the binary solvent mixture on the viscosity, a set of high-molecular-weight ethyl cellulose (CAS No. 9004-57-3, Order No. 200654, Sigma-Aldrich Corp., USA) mixtures with different BCA-to-xylene weight ratios were considered. As shown in Fig. 10(b), the high-molecular-weight ethyl cellulose solution with a BCA-to-xylene weight ratio of 4:1 exhibited the lowest viscosity.

In addition to the aforementioned conventional measures, metallorganic silver, which can be dissolved in the binary solvent mixture, was employed as a novel measure to control the viscosity of the bimodally dispersed silver paste. Interestingly, the addition of metallorganic silver decreased the viscosity of the bimodally dispersed silver paste, as shown in Fig. 10(c). The used metallorganic silver,

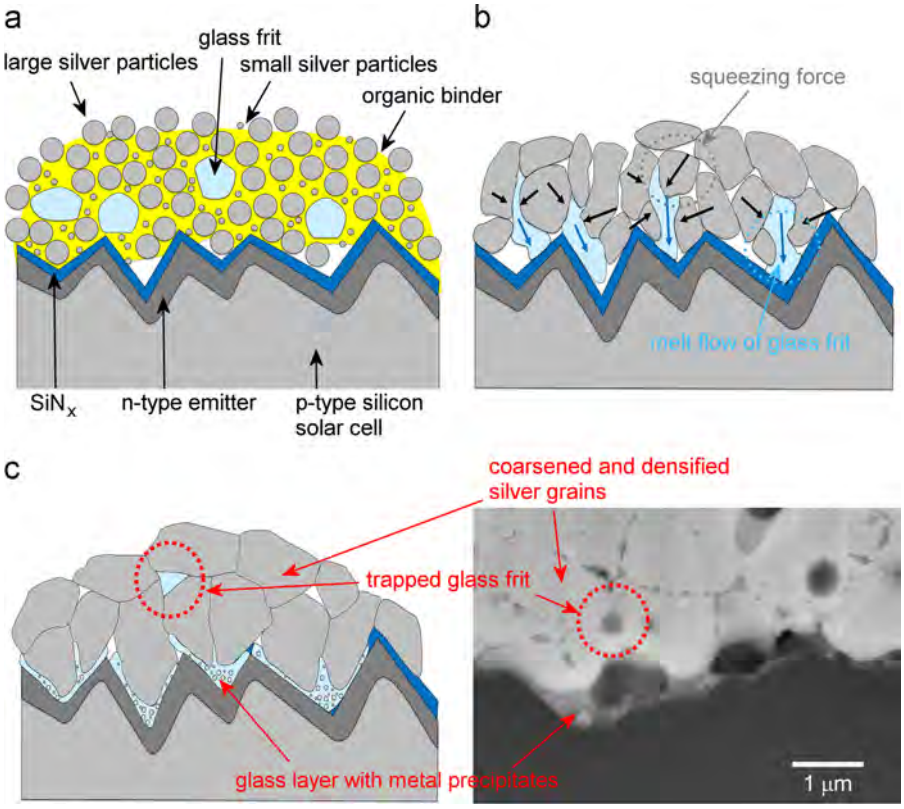

Fig. 6. The melt flow mechanism of glass frit: (a) dried silver paste, (b) melt flow of glass frit due to the densification and coarsening of silver particles, and (c) fired silver electrode with trapped glass frit.

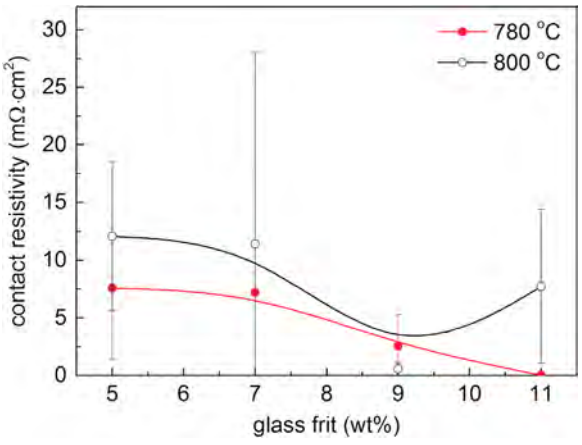

Fig. 7. Contact resistivity versus the solid content of glass frit in the bimodally dispersed silver paste (HP0702:HP0710=1:4).

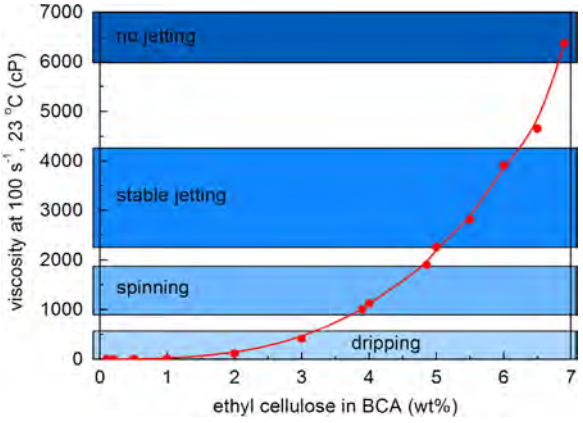

Fig. 8. EHD-jetting characteristics along with ink viscosity.

which has a similar molecular structure to the carboxylic-acid-based dispersant, is postulated to adsorb on the silver particle surface if there is no polymeric dispersant present, hence reducing the viscosity of the bimodally dispersed silver paste. Moreover, the use of metallorganic silver in the bimodally dispersed silver paste contributes to not only the decrease of the electrical resistivity because it eventually turns into a metallic state after thermal decomposition [25–27] but also the reduction of contact resistivity due to the noble-metal-assisted etching capability [28].

3.3. Fabrication of a polycrystalline silicon solar cell using EHD jet printing

Finally, the bimodally dispersed silver paste was tuned to have a viscosity of approximately 4200 cP at the shear strain rate of $100\ s^{-1}$ by adding 5 wt% of metallorganic silver. The bimodally dispersed silver paste was printed using an EHD jet printer on polycrystalline silicon solar cell wafers with an emitter sheet resistance of 60 Ω/sq (Hanwha Chemical R&D Centre, Republic of Korea), which was common in 2010 and the average cell efficiency was approximately 16.5% [29]. However, the bimodally dispersed silver paste with the mixture of BCA and xylene presented two major problems: (1) it dried too quickly at the nozzle tip, and (2) it spread excessively on the textured surface of a polycrystalline silicon solar cell wafer. Therefore, the mixture of BCA and xylene at the weight ratio of 4 to 1 was replaced with a mixture of BCA and α-terpineol at the weight ratio of 1 to 1 because α-terpineol not only has a high boiling point but can also dissolve metallorganic silver. As shown in Fig. 11, the bimodally dispersed silver paste with the mixture of BCA and α-terpineol exhibited much less spreading

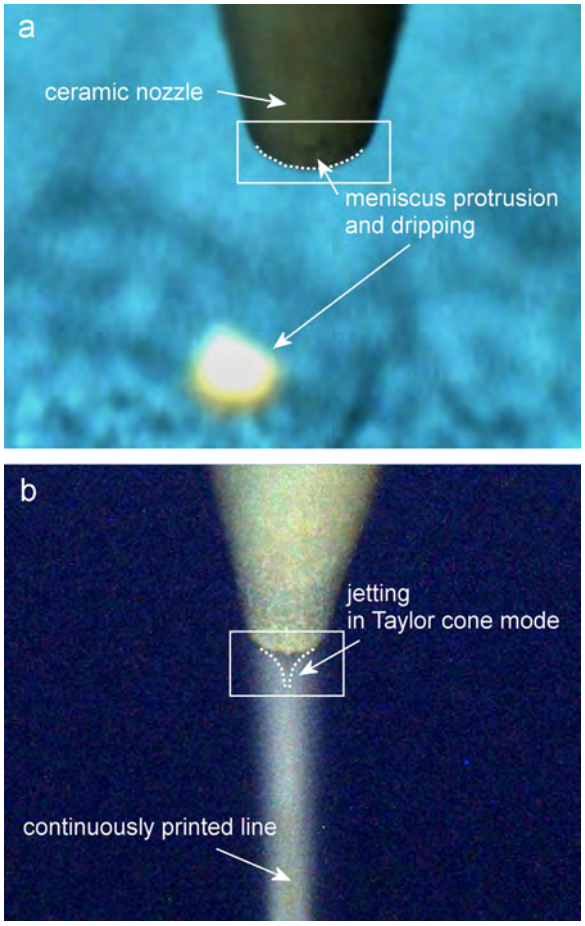

Fig. 9. EHD-jetting behaviours with (a) low viscosity ink, and (b) optimal viscosity ink.

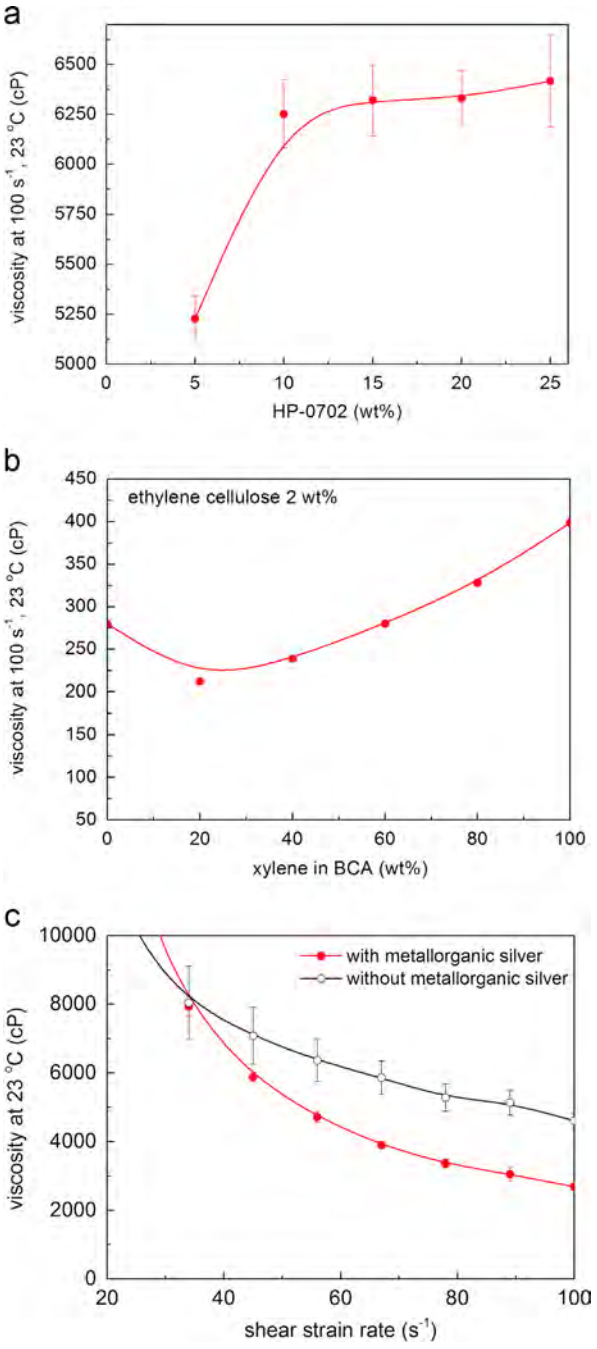

Fig. 10. Viscosity dependence on (a) the weight ratio of small-to-large silver particles in the bimodally dispersed silver paste, (b) the weight ratio of xylene-to-BCA in the binary solvent mixture, and (c) the 2.5 wt% addition of metallorganic silver with respect to the silver particles and glass frit.

and spattering around the EHD jet printed line compared to that with the mixture of BCA and xylene. To further restrain the spreading of the bimodally dispersed silver paste, the heating platen temperature was set 60 °C to evaporate the carrier vehicle as quickly as possible.

The EHD jet printing was conducted 30 times at the printing speeds of 5 cm/s and 10 cm/s. The typical standoff distance between the nozzle tip and a polycrystalline silicon solar cell wafer was set at approximately 0.5 mm. The applied voltage and flow rate fell in the range of 1.3–1.4 kV and 0.3–0.4 μl/min, respectively. The resulting line height and width of the EHD jet printed silver electrodes were approximately 51.50 μm and 60 μm, respectively, as shown in Fig. 12(b). As shown in Table 1 where reference cell efficiencies with the similar emitter sheet resistance in 2010 are listed, the resulting cell efficiency of the EHD jet printed polycrystalline silicon solar cell with the finger spacing of 2 mm reached up to 16.72%, which is higher than that of screen-printed cells by +0.22–0.52%p [7,8,15] but slightly lower than that of a dispensing printed cell by −0.05%p [8] which might be below measurement uncertainties on polycrystalline silicon solar cells. Compared to the cell efficiency of an EHD jet printed polycrystalline silicon solar cell with diluted commercially available silver paste for screen-printing, the bimodally dispersed silver paste, optimized for EHD-jet printing, greatly improved the cell efficiency by +3.02%p [15].

However, the EHD jet printed polycrystalline silicon solar cell exhibits a bit low fill factor, when the measured unit-line resistance and contact resistivity in Fig. 5(a) and Fig. 7 are considered. Because the developed silver paste had much lower viscosity and yield stress than those of silver paste for screen printing, the average line width of screen-printed silver electrodes was around 350 μm, which was much wider than that of EHD jet printed silver electrodes. As a result, the unit-line resistance of EHD jet printed silver electrodes must be higher. Moreover, the contact resistivity on polycrystalline silicon solar cell wafers with the emitter sheet resistance of 60 Ω/sq must be higher than that on monocrystalline silicon solar cell wafers with the emitter sheet resistance of 50 Ω/sq. In addition, the inhomogeneous distribution of glass frit might lead to the non-uniform etching of the SiN_x layer since the D50 and D90 values of the used glass frit were 4.52 μm and 10.11 μm, respectively, and they

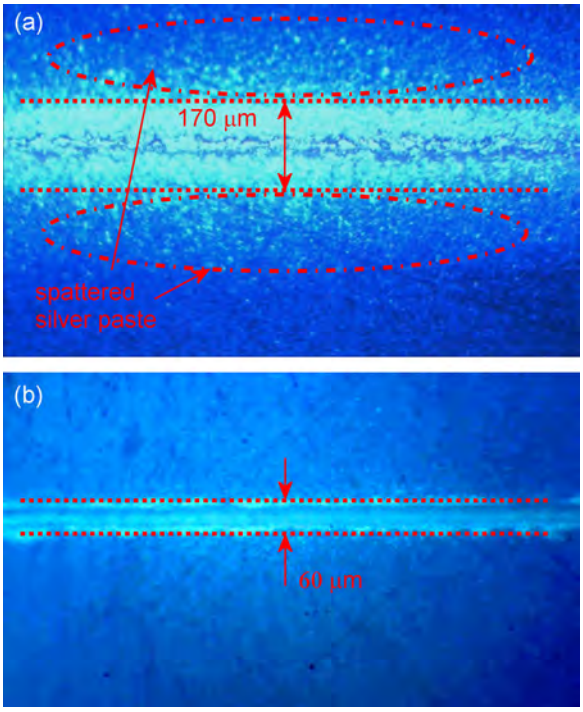

Fig. 11. Comparison of EHD jet printed lines using the bimodally dispersed silver paste with the mixture of (a) BCA and xylene and (b) BCA and α-terpineol.

might be too big for fine silver electrodes. The increased unit-line resistance and contact resistivity consequently increased series resistance and hence might reduce the fill factor of the EHD jet printed polycrystalline silicon solar cell.

3.4. *Issues for the advancement of EHD jet printed crystalline silicon solar cells*

Despite the successful experimental results of EHD jet printed polycrystalline silicon solar cells with the bimodal dispersed silver paste, there are a couple of challenging issues for its further advancement. The most imminent issue is the strong necessity to reduce the number of EHD-jet printings for high height-to-width aspect ratio silver electrodes. Although it might not be possible to achieve such high height-to-width aspect ratio silver electrodes by single pass printing, the number of EHD-jet printings should be greatly reduced from 30 times in this study to a couple of times from the industrial production viewpoint. This issue inevitably implies that the deposition rate of EHD-jet printing should be higher by a factor of ten and above. For achieving this goal, the as-printed silver electrode must hold its shape rather than spread on a crystalline silicon solar cell wafer. Three possible solutions might be conceivable; (1) EHD-jet printing of silver paste containing a volatile carrier vehicle might be helpful. However, the use of a highly volatile carrier vehicle might lead to a nozzle clogging problem; (2) the increase of yield stress of silver paste with a rheological modifier might help to hold the shape of an as-printed silver electrode. However, suppressing the viscosity increase of silver pate due to the use of a rheological modifier might be challenging; (3) the use of phase changeable or UV curable silver paste might be a more realistic solution. Hotmelt paste, which liquefies on a hot screen but quickly solidifies on a crystalline silicon solar cell wafer, was already demonstrated by using screen printing [30]. Moreover, UV curable silver paste has been used in printed electronics applications. This approach also has its own challenge as like the aforementioned conceivable solutions. In the case of hotmelt paste, as-printed silver electrodes should not collapse nor spread by melting in the course of firing. In the case of UV curable silver paste, the development of a UV curable material with a minimal residue after firing is required.

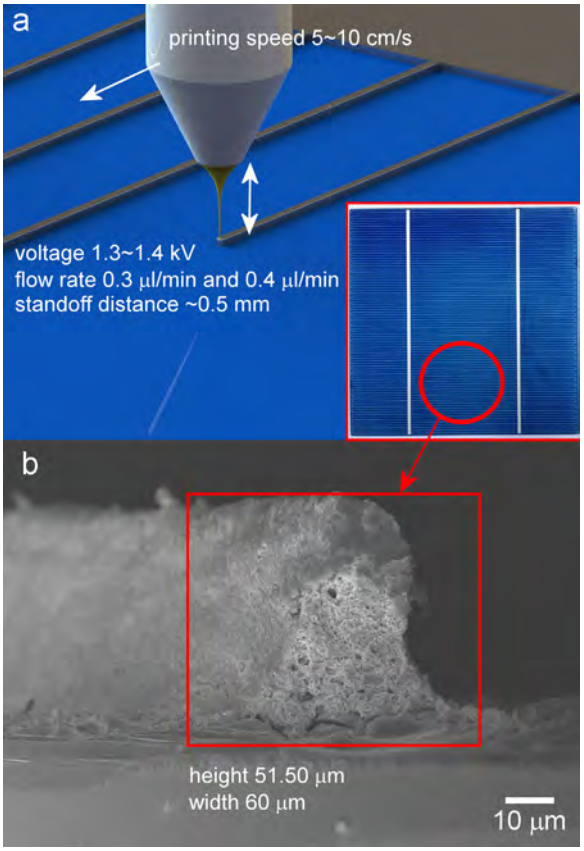

Fig. 12. (a) EHD jet printed polycrystalline silicon solar cell, and (b) the cross-sectional SEM image of a silver electrode.

4. Conclusions

In this study, the electrical and rheological characteristics of the bimodally dispersed silver particles in silver paste were systematically investigated for EHD jet printing. With an increase in the weight ratio of small-to-large silver particles, the unit-line resistance consistently decreased. In contrast, the contact resistivity became minimal at the small-to-large silver particle weight ratio of 15 wt% but increased for higher weight ratios. This contact resistivity increase above 15 wt% was a result of the obstructed melt flow of glass frit because of the narrow passages between necked silver particles. Moreover, the addition of small silver particles increases the viscosity of the bimodally dispersed silver paste due to the enlarged specific surface area of the small silver particles. To tune the viscosity of the bimodally dispersed silver paste within the EHD-jettable viscosity range, a low-molecular-weight organic binder was dissolved in a binary solvent mixture. In addition, metallorganic silver was effective for reducing the viscosity of the bimodally dispersed silver paste because of the molecular structural similarity of the used metallorganic silver to the carboxylic-acid-based dispersant. With the developed bimodally dispersed silver paste for EHD jet printing, silver electrodes with the height-to-width aspect ratio of 0.86 could be printed, and the cell efficiency of the resulting polycrystalline silicon solar cell reached 16.72%, which was an improvement over EHD jet printing with diluted commercially available silver paste by +3.02%p. The unique traits of EHD jet printing, *i.e.*, the construction of fine but high height-to-width

Table 1
Cell efficiency comparison of polycrystalline silicon solar cells with the similar emitter sheet resistance.

Printing method	J_{sc} (mA/cm^2)	V_{oc} (mV)	Fill factor (%)	Efficiency (%)	Reference
EHD jet printing with the bimodally dispersed silver paste	34.61	616.8	78.3	16.72	
EHD jet printing with the dilute version of commercially available silver paste	32.98	608	68.1	13.7	[15]
Dispensing printing	34.47	616.22	78.99	16.77	[8]
Ink-jet printing	32.2	592.9	63.6	12.1	[7]
Reference cell using conventional screen-printing	34.8	615.3	77.2	16.5	[7]
	33.8	615.97	79.11	16.47	[8]
	34.19	610	77.8	16.2	[15]

aspect ratio silver electrodes with a relatively large diameter nozzle, will significantly improve the front-side metallization in crystalline silicon solar cell applications.

Acknowledgements

This work was supported by grants awarded under the New & Renewable Energy Technology Development Program of the Korea Institute of Energy Technology Evaluation and Planning funded by the Korean Ministry of Knowledge Economy (Grant No. 20113020010060), the Research and Development Program of the Korea Institute of Energy Research (Grant No. B4-2422), and the Basic Science Research Program of the National Research Foundation of Korea funded by the Ministry of Education, Science and Technology (Grant No. 2012R1A1A2038889).

References

[1] S. Honghang, Z. Qiang, W. Yibo, Y. Qiang, S. Jun, China's solar photovoltaic industry development: the status quo, problems and approaches, Appl. Energy 118 (2014) 221–230.
[2] T. Saga, Advances in crystalline silicon solar cell technology for industrial mass production, NPG Asia Mater 2 (2010) 96–102.
[3] A. Mette, P.L. Richter, M. Hörteis, S.W. Glunz, Metal aerosol jet printing for solar cell metallization, Prog. Photovoltaics 15 (2007) 621–627.
[4] M. Hörteis, S.W. Glunz, Fine Line Printed, Silicon solar cells exceeding 20% efficiency, Prog. Photovoltaics 16 (2008) 555–560.
[5] D.-Y. Shin, Fabrication of an inkjet-printed seed pattern with silver nanoparticulate ink on a textured silicon solar cell wafer, J. Micromech. Microeng 20 (2010) 125003.
[6] Y.T. Gizachew, L. Escoubas, J.J. Simon, M. Pasquinelli, J. Loiret, P.Y. Leguen, J.C. Jimeno, J. Martin, A. Apraiz, J.P. Aguerre, Towards ink-jet printed fine line front side metallization of crystalline silicon solar cells, Sol. Energy Mater. Sol. Cells 95 (2011) S70–S82.
[7] D.-Y. Shin, Y.-K. Cha, H.-H. Ryu, S.-H. Kim, Impact of effective volume ratio of a dispersant to silver nano-particles on silicon solar cell efficiency in direct ink-jet metallization, J. Micromech. Microeng 22 (2012) 115007.
[8] M. Pospischil, K. Zengerle, J. Specht, G. Birkle, P. Koltay, R. Zengerle, A. Henning, M. Neidert, C. Mohr, F. Clement, D. Biro, Investigations of thick-film-paste rheology for dispensing applications, Energy Procedia 8 (2011) 449–454.
[9] D.-H. Kim, S.-S. Ryu, D. Shin, J.-H. Shin, J.-J. Jeong, H.-J. Kim, H.S. Chang, The fabrication of front electrodes of Si solar cell by dispensing printing, Mater. Sci. Eng. B 177 (2012) 217–222.
[10] M. Pospischil, M. Klawitter, M. Kuchler, J. Specht, H. Gentischer, R. Efinger, C. Kroner, M. Luegmair, M. König, M. Hörteis, C. Mohr, L. Wende, J. Lossen, M. Weiß, O. Doll, I. Koehler, R. Zengerle, F. Clement, D. Biro, Process development for a high-throughput fine line metallization approach based on dispensing technology, Energy Procedia 43 (2013) 111–116.
[11] J.H. Lee, Y.H. Lee, J.Y. Ahn, J.-W. Jeong, Analysis of series resistance of crystalline silicon solar cell with two-layer front metallization based on light-induced plating, Sol. Energy Mater. Sol. Cells 95 (2011) 22–25.
[12] J.-U. Park, M. Hardy, S.J. Kang, K. Barton, K. Adair, D.K. Mukhopadhyay, C.Y. Lee, M.S. Strano, A.G. Alleyne, J.G. Georgiadis, P.M. Ferreira, J.A. Rogers, High-resolution electrohydrodynamic jet printing, Nat. Mater. 6 (2007) 782–789.
[13] T. Sekitani, Y. Noguchi, U. Zschieschang, H. Klauk, T. Someya, Organic transistors manufactured using inkjet technology with subfemtoliter accuracy, Proc. Natl. Acad. Sci. U.S.A 105 (2008) 4976–4980.
[14] J.-A. Jeong, H.-K. Kim, J. Kim, Invisible Ag grid embedded with ITO nanoparticle layer as a transparent hybrid electrode, Sol. Energy Mater. Sol. Cells 125 (2014) 113–119.
[15] Y. Jang, I.H. Tambunan, H. Tak, V.D. Nguyen, T. Kang, D. Byun, Non-contact printing of high aspect ratio Ag electrodes for polycrystalline silicone solar cell with electrohydrodynamic jet printing, Appl. Phys. Lett. 102 (2013) 123901.
[16] P.N. Vinod, B.C. Chakravarty, M. Lal, R. Kumar, S.N. Singh, A novel method for the determination of the front contact resistance in large area screen printed silicon solar cells, Semicond. Sci. Technol. 15 (2000) 286–290.
[17] P.N. Vinod, Specific contact resistance measurements of the screen-printed Ag thick film contacts in the silicon solar cells by three-point probe methodology and TLM method, J. Mater. Sci. Mater. Electron 22 (2011) 1248–1257.
[18] P.N. Vinod, The electrical and microstructural properties of electroplated screen-printed Ag metal contacts in crystalline silicon solar cells, RSC Adv 3 (2013) 14106–14113.
[19] X. Wu, R.D. Oleschuk, N.M. Cann, Characterization of microstructured fibre emitters: in pursuit of improved nano electrospray ionization performance, Analyst 137 (2012) 4150–5161.
[20] S. Magdassi, The Chemistry of Inkjet Inks, World Scientific Publishing Co., Singapore, 2009.
[21] P. Boch, J. Nièpce, Ceramic Materials: Processes, Properties, and Applications, Wiley-ISTE, 2007.
[22] M.M. Hilali, K. Nakayashiki, C. Khadilkar, R.C. Reedy, A. Rohatgi, A. Shaikh, S. Kim, S. Sridharan, Effect of Ag particle size in thick-film Ag paste on the electrical and physical properties of screen printed contacts and silicon solar cells, J. Electrochem. Soc. 153 (2006) A5–A11.
[23] S.Y. Kim, S.J. Kim, S.S. Jee, J.M. Park, K.H. Park, S.C. Park, E.A. Cho, J.H. Lee, I.Y. Song, S.M. Lee, I.T. Han, K.R. Lim, W.T. Kim, J.C. Park, J. Eckert, D.H. Kim, E.-S. Lee, Capillary flow of amorphous metal for high performance electrode, Sci. Rep 3 (2013) 2185.
[24] R. Greenwood, P.F. Luckham, T. Gregory, The effect of diameter ratio and volume ratio on the viscosity of bimodal suspensions of polymer lattices, J. Colloid Interface Sci. 191 (1997) 11–21.
[25] C.-A. Lu, P. Lin, H.-C. Lin, S.-F. Wang, Effects of metallo-organic decomposition agents on thermal decomposition and electrical conductivity of low-temperature-curing silver paste, Jpn. J. Appl. Phys. 45 (2006) 6987–6992.
[26] C.-A. Lu, P. Lin, H.-C. Lin, S.-F. Wang, Characterization of the low-curing-temperature silver paste with silver 2-ethylhexanoate addition, Jpn. J. Appl. Phys. 46 (2007) 251–255.
[27] D.-Y. Shin, M. Jung, S. Chun, Resistivity transition mechanism of silver salts in the next generation conductive ink for a roll-to-roll printed film with a silver network, J. Mater. Chem. 22 (2012) 11755–11764.
[28] D.-Y. Shin, J.-Y. Seo, M.G. Kang, H.-E. Song, Contact resistivity decrease at a metal/semiconductor interface by a solid-to-liquid phase transitional metallo-organic silver, ACS Appl. Mater. Interfaces 6 (2014) 15933–15941.
[29] SEMI P.V. Group 2012, International Technology Roadmap for Photovoltaic (ITRPV.net), Results 2011, ⟨http://www.itrpv.net/.cm4all/iproc.php/Reports%20downloads/roadmap_itrpv_march_2012_full_web.pdf⟩, last accessed on the 23rd October, 2014.
[30] A. Mette, D. Pysch, G. Emanuel, D. Erath, R. Preu, S.W. Glunz, Series resistance characterization of industrial silicon solar cells with screen-printed contacts using hotmelt paste, Prog. Photovoltaics 15 (2007) 493–505.